Agnieszka LISOWSKA-LIS[1], Franciszek WITOS[2]

10. THE USE OF THERMOGRAPHY TO IMPROVE THE SAFETY OF ELECTRICAL DEVICES IN THE POWER INDUSTRY

10.1. Introduction

Temperature measurement and early detection of local increase in the surface temperature may be crucial for the power system machinery and equipment as indication of failure or its improper work. Thermal cameras used for monitoring can easily detect increase of the surface temperature of electrical equipment. Since the 2000s, industry guidelines and international standards have been introduced for the testing of electrical and mechanical equipment using infrared thermography [1, 2, 3, 4, 5, 6, 7].

Thermography (thermovision) was used in the power industry as early as the 1960s. Losses in large power devices such as power transformers were investigated using AGAMA cameras cooled with liquid nitrogen. With thermovision it is possible to detect local temperature increases (“hot spots”) in: power devices at power stations and substations, electrical power lines, power cables, connections, etc. [1, 4, 5, 6, 7]. Since the 1980s, thermal imaging cameras with a design based on uncooled microbolometric detectors from companies such as FLIR or FLUKE have been popular. They have become more common in use as they are small, portable and relatively cheap. Thermography is a method of detecting damage or faulty operation of equipment in the power industry. This method supports and complements the regular visual inspection of equipment and the obligatory standardized methods of diagnostics of power devices. Thermal imaging enables quick detection of potential damage areas. During the measurement, it is not necessary to disconnect the tested device from the power supply. The basis for the detection of potential damage is the observation of: "hot spots" in the uniform temperature distribution on the surface of the equipment, and abnormal increase in temperature of the device surface [5, 6, 7, 8, 9, 10, 11].

[1] Department of Electrical Engineering, Polytechnic Faculty, University of Applied Sciences in Tarnow, Mickiewicza 8, 33-100 Tarnów, Poland, lisowskalis@pwsztar.edu.pl
[2] Department of Optoelectronics, Faculty of Electrical Engineering, Silesian University of Technology, ul. Krzywoustego 2, 44-100 Gliwice, Poland, franciszek.witos@polsl.pl

The basic radiometric quantities used in the analysis of infrared radiation of objects are: the energy exitance and the energy luminance. The energy exitance, or emissivity, is the surface density of the radiant energy flux Φ from the surface S to the half-space. The energy luminance is the surface density of the radiant energy flux Φ from the surface S, in the unit of spatial angle $d\Omega$. The above values can be related to the elementary spectral range ($d\lambda$), or spectral densities. The **monochromatic radiant exitance** from the surface of the black body, around a given wavelength, according to the Lambert's cosine law and the Planck's law [2, 12], is equal to:

$$M_{e,\lambda} = \frac{dM_e}{d\lambda} = \frac{2\pi hc^2}{\lambda^5(e^{\frac{hc}{\lambda kT}} - 1)} [\mathrm{W} \cdot \mathrm{m}^{-2} \cdot \mu\mathrm{m}^{-1}], \quad (1)$$

where:

$M_{e,\lambda}$ – monochromatic radiant exitance [$\mathrm{W} \cdot \mathrm{m}^{-2} \cdot \mu\mathrm{m}^{-1}$];

M_e – power emitted [W];

λ – wavelength [$\mu\mathrm{m}^{-1}$];

T – temperature of that surface[K];

k – the Boltzmann constant;

c – the speed of light in the medium.

The physical body properties are described by the emissivity coefficient, expressed as ε. The emissivity of real bodies represents the ratio of the power emitted M_e from the surface of a given body to the total power of radiation incident on this body M_p

$$\varepsilon = \frac{M_e}{M_p} \quad (2)$$

where:

M_e – power emitted [W];

M_p – the total power of radiation incident on this body [W].

A black body is an object whose surface has the greatest emissivity value, $\varepsilon = 1$. This means that such an object emits all radiation incident on this body. Such a case is purely theoretical, it does not occur in nature [2, 12].

10.2. Thermovision applied for the safety of electrical power system - detection of surface temperature increase

The basis for the detection of potential damage is the observation of: "hot spots" in the uniform temperature distribution on the surface of the equipment or the contact surface, abnormal increase in temperature of the device surface in relation to the ambient temperature, and the appearance of differences in the temperature distribution of devices powered from three

phases [5, 6, 7]. Figure 1 presents three wires: L1, L2, L3 (the same line and voltage, similar current). The analysis shows their proper state. Elements in all three phases have similar temperature.

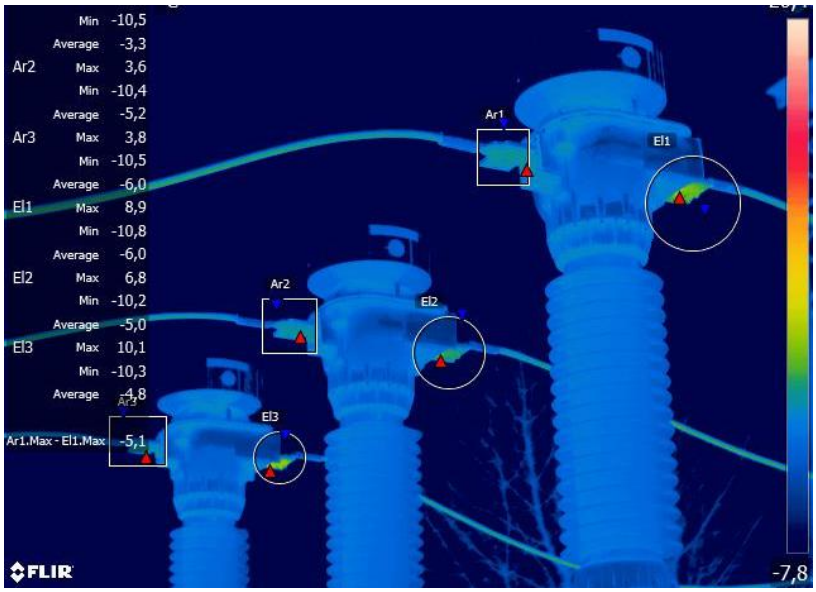

Fig. 1. The thermogram shows the wiring connections in three current transformers (Un = 110 kV), three phases L1, L2, L3. The thermogram was made with a FLIR P640 camera

Rys. 1. Termogram przedstawia połączenia przewodów trzech faz L1, L2, L3 z przekładnikami prądowymi (Un = 110 kV). Wykonano kamerą termowizyjną FLIR P640

The thermovision method enables **control of the operation** of generators, transformers, power boilers, lines, switchboards and other electrical power devices [2, 6, 7]. Regular diagnostics of high-voltage (HV) devices and damage detection are aimed at maintaining their operational reliability. Maintaining the proper operating conditions of the device reduces degradation processes, and thus extends its life [2, 6, 7, 13].

The most expensive devices in a power system are power transformers. Constant monitoring and periodical tests must be done to maintain best condition of this equipment and to avoid a power system breakdown. In the case of power oil transformer tests an important role is played by tests performed without disconnecting the transformer from the power system. These are: chromatographic analysis of gases dissolved in transformer oil (DGA), tests of partial discharges (PDs) by electrical, acoustic, chemical, and optical methods, tests of magnetization processes, vibro-acoustic analysis, and thermal imaging studies. Combined power transformer testing methods have recently been developed. The **acoustic emission done simultaneously with thermal imaging** provides better results of the power transformer failure detection [9].

An untypical **transformer** surface overheating or an untypical temperature distribution on the surface might be evidence of the deterioration of machinery elements (winding, core, connections and clamps). The fastest deterioration occurs for the electrical insulation (paper, oil). Surface overheating can also be evidence of improper ambient or work conditions.

Disruptions or failures in a power system affect the transformer work parameters. For a transformer in good condition, the lower areas on the surface should be cooler. It was observed that for transformers with deteriorated electrical insulation (Fig. 2) the maximum temperature areas ("hot-spots") could be observed on any surface [8, 11].

Fig. 2. The thermogram presents transformer with ineffective cooling. The surface temperature is almost even, despite the working fans and cooling circulation (autotransformer: 220/110/15 kV, 160 MVA). The thermogram was made with a FLIR E50 camera

Rys. 2. Termogram przedstawia transformator którego chłodzenie nie jest skuteczne. Rozkład temperatury na powierzchni jest prawie jednakowy, mimo działających wentylatorów oraz wymuszenia obiegu chłodzenia (autotransformator: 220/110/15 kV, 160 MVA). Wykonano kamerą termowizyjną FLIR E50

The higher temperature on the entire upper surface of the transformer tank is justified by all possible processes responsible for the generation of heat within the working transformer. On Figs. 3 and 4 local temperature increase due to **improper state of junction or improper wires connection** was observed. The thermogram in Fig. 3 shows uneven temperature distribution on the screw joint (a). Detailed analysis Fig. 3b demonstrates that the temperature difference between the screws reaches 10°C. This could be due to a loose screw and eddy currents.

a) b)

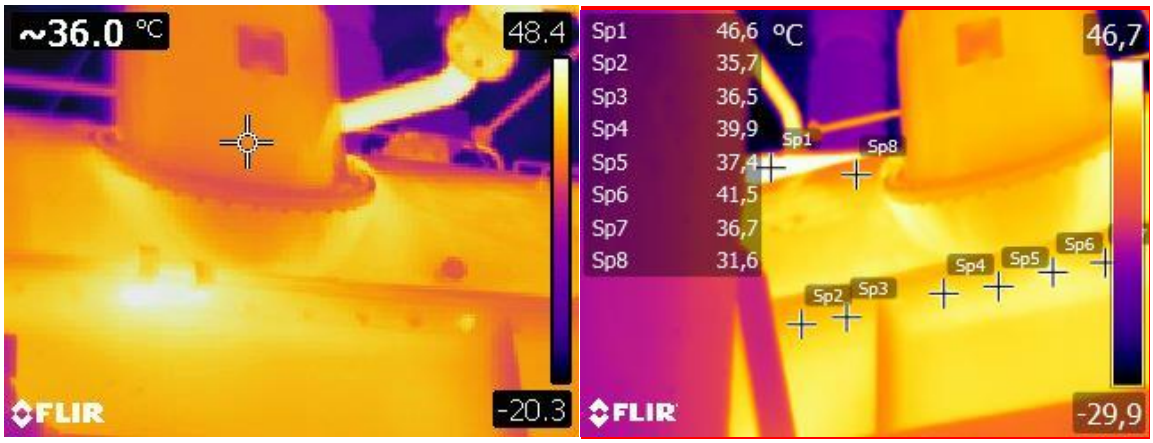

Fig. 3. The thermogram shows the uneven temperature distribution on the screw joint (a). Detailed analysis (b) shows that temperature difference between the screws reaches 10°C (autotransformer: 220/110/15 kV, 160 MVA). This could be due to a loose screw and eddy currents. The thermogram was made with a FLIR E50 camera

Rys. 3. Termogram przedstawia niejednorodny rozkład temperatury połączeń śrubowych (a). Szczegółowa analiza (b) pokazuje, że różnica temperatur śrub osiąga 10°C (autotransformator: 220/110/15 kV, 160 MVA). Przyczyną może być osłabione połączenie śrubowe, przepływ prądów wirowych. Wykonano kamerą termowizyjną FLIR E50

Fig. 4. The thermogram shows the slightly higher temperature for the wire and isolation at the 110 kV voltage side of power transformer (autotransformer: 220/110/15 kV, 160 MVA). The thermogram was made with a FLIR E50 camera

Rys. 4. Termogram ujawnia nieco podwyższoną temperaturę przewodów oraz izolacji przepustów po stronie 110 kV dla transformatora mocy (220/110/15 kV, 160 MVA). Wykonano kamerą termowizyjną FLIR E50

The temperature increase is associated with an increase in the connection resistance. The reasons for this may be defects or damage to the structure, loose screws, corrosion, oxidation, improper connection and others [2, 5, 6, 8, 13]. In electrical power stations and substations, the

middle voltage (MV) devices as well as the low voltage (LV) devices may be tested using an infrared camera (LV means U_N=220 V (in older systems but still in use), or 230 V (in new ones)). Figure 5 presents thermograms of a **LV equipment** (220 V) at a power station. The thermogram shows the detection of an abnormal state of low voltage circuit breakers. The observed increase in surface temperature was due to poor connection of wires and cracks in ceramic insulators.

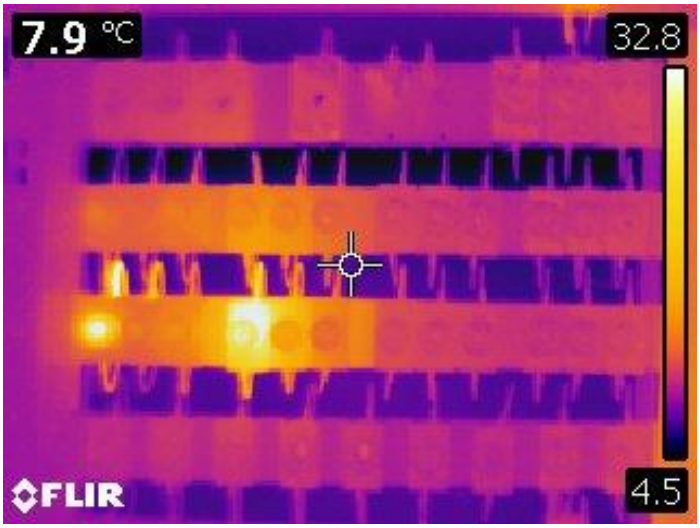

Fig. 5. The thermogram shows the detection of an abnormal state of low voltage circuit breakers. The observed increase in surface temperature was due to poor connection of wires and cracks in ceramic insulators. Electrical substation, LV equipment (220 V). The thermogram was made with a FLIR E50 camera

Rys. 5. Termogram umożliwił detekcję uszkodzeń bezpieczników niskich napięć. Zaobserwowany wzrost temperatury był spowodowany poluzowanym połączeniem przewodów oraz pęknięciem ceramicznej obudowy izolacyjnej. Stacja energetyczna, sprzęt po stronie nn (220 V). Wykonano kamerą termowizyjną FLIR E50

Damage detection in the power industry is crucial. To prevent breakdowns, power generation, transmission and distribution companies carry out technical inspections of power equipment every two years, while high voltage power lines are inspected every year or every two years [6, 7, 11]. In 2010 - 2020, energy and distribution companies monitored high voltage power lines using thermal imaging cameras. Such inspections are conducted also with helicopters or drones, which speeds up observation. This led to a significant reduction of a number of network failures [6, 7, 11].

Another kind of equipment that might be tested for failures with thermal imaging cameras are **surge arresters**. They are very efficient devices applied for protection of high voltage and medium voltage electrical equipment (transformers, circuit-breakers, switches, bushings, lines). They are used to eliminate the effect of overvoltage (i.e. lightning strike, electrostatic discharge, electromagnetic pulse). They also stop the current from the surge caused by switching operation in the power system discharge. The current from the surge is diverted through the arrester (usually to the ground). Effective overvoltage protection requires different surge arrester types

to be used [14, 15, 16]. Metal–oxide varistors have been used since the 1970s to limit surges in electrical networks. They are also known as variable-resistors (varistors). Varistors are manufactured on the basics of polycrystalline ZnO (about 90%) with addition of magnesium, cobalt-, bismuth- and chromium-oxides. In the medium voltage surge arrester varistors are covered in fiber-reinforced plastic tubes and silicone rubber sheds are directly molded on them [14, 15]. Varistor resistance is maximal. The leakage current strongly depends on varistor temperature [17, 18]. The surface temperature changes in time correlate with the energy generated inside the varistors [17, 18, 19, 20]. This process can be computed or modelled for the safety analysis of the whole surge arrester [21, 22]. In continuous operation, the arrester provides no (or minimal) current. In the case of operating duty, i.e., during a lightning or switching energy impulse, the discharge current flows. The arrester limits the voltage to the residual voltage level (indicated in the arrester specification as: U_{res}). The measurement of the reference voltage U_r (at the reference current) and residual voltage (at the nominal discharge current) ensures a control of the $U = f(I)$ characteristic of surge arrester. The construction of the surge arrester provides mechanical isolation of varistors to protect the fragile polycrystalline elements (in polymer tube housing and silicone rubber outer cover). Those parts of arrester must transmit effectively thermal radiation from varistors; Generally they are not as efficient as metal radiators. Stabilization process is repetitive. After cooling, the arrester may return to the stable operating point. If effective factors on the heat transfer coefficient are considered constant, heat dissipation ability may be approximated as a linear function up to 100°C. In that range the arrester parts are in thermal balance, which means that the arrester surface temperature vs. thermal power loss characteristics is quasi-linear [14, 16, 17]. If the energy is too high, it leads to destruction of the varistor micro- or macrostructure. The current flowing through the varistor increases rapidly and finally the varistor does not stabilize the voltage any more. Electrical energy leads to increase in thermal energy generated. Without effective energy dissipation rapid destruction of varistor occurs. The effect may be varistor explosion [14, 16, 17]. Varistors are tested before exploitation to confirm stable operational properties (with AC, impulse current, or DC). The producer declares nominal discharge current (for 8/20 μs pulse) I_N (in kA), continuous operating voltage U_C (in V), voltage protection level U_{PN} [V], at I_N and maximal partial discharges (in pC). [14, 16]. Emissivity coefficient (ε) of the matt silicone rubber is high, about 0.97 [2, 11, 13]. That provides excellent conditions for the surface varistor temperature analysis using thermal cameras. The IR camera can be used to detect the faults of ZnO metal – oxide surge arresters that lead to an increase in surface temperature [11]. Recently some researches have been dedicated to analysing arrester surface temperature and leakage current, or the state of the arresters. Novizon and co-workers [23] analysed correlation with third harmonic resistive leakage current and condition of ZnO arrester. Some analysis of power loss problems, degradation of varistors and temperature changes was done both in the laboratory and in the field searches [24, 25].

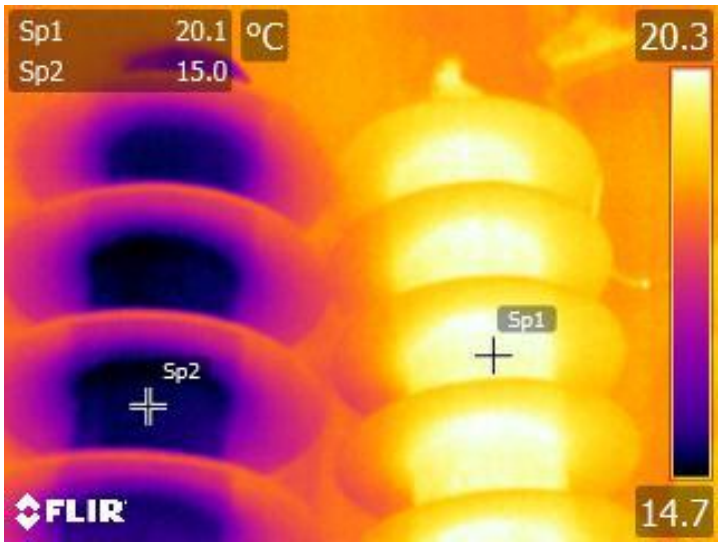

Fig. 6. Thermograms of metal–oxide surge arresters (MOA): one before (left) and one after the testing (right). The MOA right was tested during 10 min. at voltage $U = U_C = 18$ [kV] and registered leakage current was $I_{arr} = 0.6$ [mA], [source: 11]

Rys. 6. Termogram przedstawia warystorowe ograniczniki przepięć: przed testem (lewy) oraz po zakończeniu testu (prawy). Ograniczniki były badane przez 10 min. pod napięciem $U = U_C = 18$ [kV] a zarejestrowany prąd upływu wynosił $I_{arr} = 0.6$ [mA], [source: 11]

The surface temperature of the medium voltage surge arrester correlates with an increase in leakage current Fig 6. The result shows that the 0.6 mA AC leakage current in the medium voltage metal–oxide surge arrester (18 kV) is above the stable operating point, and the loss of electrical power is higher than the effective heat dissipation in the arrester [11].

10.3. Gas leakage monitoring with thermovision

In recent years, cameras operating in the infrared ranges, in which filters and image processing enable the detection of specific gases, have been introduced. The narrow working range of the camera enables the detection of a small but intense gas evaporation or gas leak. A given type of camera works in a narrow infrared band and is dedicated to the detection of only a few selected substances. One of the gases used as insulation in power devices is sulphur-hexafluoride (SF_6). Such a gas has excellent electrical insulating properties, much better than air at atmospheric pressure. Simultaneously, it is harmful to the environment. Sulphur-hexafluoride is covered by the environmental protocol. Its use is subject to restrictions and users must monitor the condition of the equipment and prevent accidental emissions. Switchgears with SF_6 gas insulation have been produced since the 1960s [7, 11]. Busbars and all distribution devices are placed in hermetically sealed pipes and tanks filled with sulphur-hexafluoride at a pressure of 0.2 ÷ 0.55 MPa. SF_6 switchgears are built for voltages from 7.2 kV up to 800 kV, mostly for cooperation with cable lines. Power supply via overhead lines generates additional costs in the form of special, large SF_6-air bushings. The use of SF_6 gas allowed for changes in

the construction of switchgears, circuit breakers and other power devices. The high voltage switchgears (60 ÷ 750 kV) in SF_6 insulation are of similar size and construction as the low voltage switchgears. The size of the switchgears has decreased, which in turn allowed for the reduction of the area occupied by the installation and a better layout of the power station. A power station or substation with a gas insulation requires less space and thus it may be located in dedicated buildings. Due to hermetic housings, the entire system is independent of atmospheric pollution or degradation processes, equipment reliability is extended and maintenance requirements are reduced. Devices insulated with SF_6 require less maintenance and repair. There is less energy loss and less fire hazard. The current switching devices are built in such a way that the rates of sulphur-hexafluoride losses are kept below 0.5% per year with a tendency to continuously decrease this value [7, 11].

Within the hermetically closed equipment gas pressure must be monitored. There are also detached switches in use, without constant gas pressure monitoring. All the equipment with SF_6 insulation must be tested (constantly or periodically) for gas leakage Fig. 7. Usually it is done with chemical gas detectors. Much more effective but more expensive is the application of thermal imaging camera dedicated to specific gas detection. Measurement with a FLIR GF306 thermal imaging camera gave much better results than the test with chemical detector [26, 27]. A FLIR GF306 thermal imaging camera can record: editable thermograms, editable thermogram sequences, and recordings in MP4 (video) format [27]. Using thermographic recording in the differential, highly sensitive mode it is possible to **compare image changes in real time** (i.e. temperature gradient analysis). Thermograms are analysed in the device's memory and the displayed graph shows the areas (pixels) indicating the intensity of temperature changes over time. For the black and white temperature scale, the thermal background was grey and the intensely cooled areas were black, while the intensely heated areas were white. This mode of operation is especially helpful for investigating small SF_6 gas leaks. In professional gas detection cameras (FLIR, FLUKE), such operations are performed by logic operations. The user obtains differential images in which the presence of gas or substance vapours is more clearly visible than on the single thermogram [27]. Image analysis in cameras allows for complex logical functions or the use of the Faster-RCNN method based on an advanced convolutional neural network, i.e. artificial intelligence [26].

Fig. 7. Testing SF_6 gas leakage from an electric switch, using a chemical detector. (Switch type: ABB OHB 1539; U_N =110 kV), [photo: A. Lisowska-Lis]
Rys. 7. Badanie wyłącznika elektrycznego pod kątem ulotu SF_6 przy użyciu chemicznego detektora gazu. (Typ wyłącznika: ABB OHB 1539; U_N =110 kV), [zdjęcie: A. Lisowska-Lis]

Figure 8 presents the result of the testing SF_6 gas leakage from an electric switch, using a thermal camera FLIR GF306. The biggest advantage is that with the thermal camera such detection was done from the distance, and the leakage could be observed at once. A sequence of thermograms was recorded in which the gas escaping could be seen. In Fig. 7 the leaking areas are marked in red for easier verification.

New techniques improve the safety of electrical devices in the power industry, because they make it possible to detect faulty operation of devices and to detect emissions of harmful or hazardous substances (including gases).

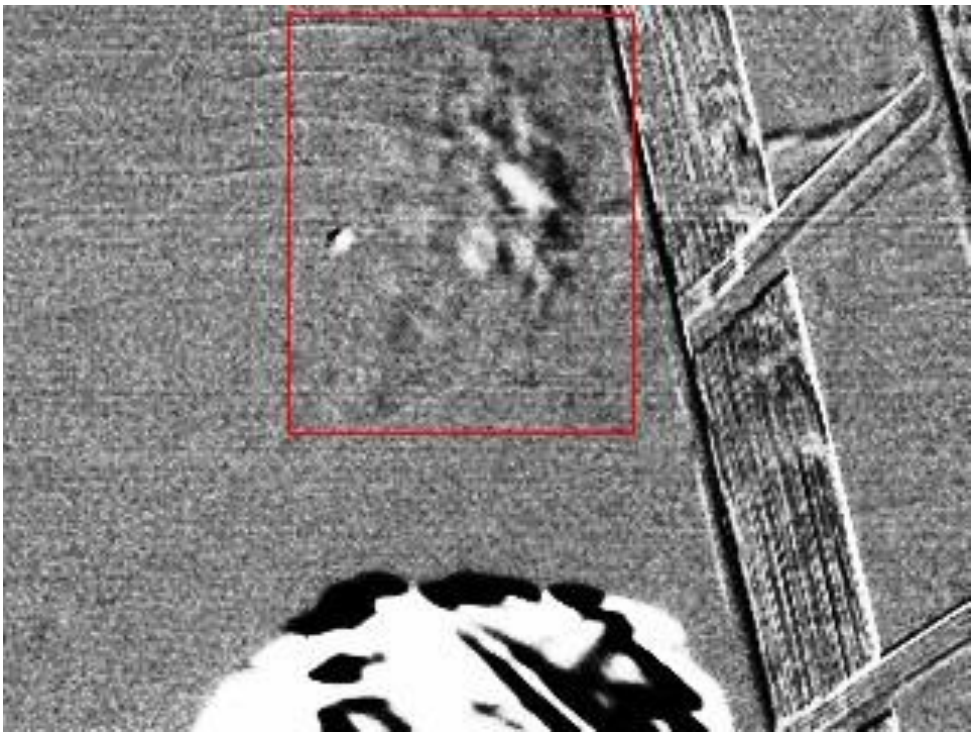

Fig. 8. Testing SF_6 gas leakage from an electric switch, using a thermal camera FLIR GF306. (Switch type: ABB OHB 1539; U_N=110 kV]

Rys. 8. Wykrycie ulotu gazu SF_6 z wyłącznika elektrycznego przy użyciu kamery termowizyjnej FLIR GF306. (Typ wyłącznika: ABB OHB 1539; U_N =110 kV)

Bibliography

1. Introduction to thermography. American Technical Publishers, Inc., Fluke Corporation and The Snell Group. Illinois 2009.
2. Więcek B., DeMey G.: Termowizja w podczerwieni, podstawy i zastosowania [in Polish]. PAK, Warszawa 2011.
3. ISO 18434-1:2008. Condition monitoring and diagnostics of machines. Thermography.
4. ASTM E1934-99a(2014), Standard Guide for Examining Electrical and Mechanical Equipment with Infrared Thermography, ASTM International, West Conshohocken, PA 2014, accessed 25.02.2020 [at]: www.astm.org.
5. Madura H.: Pomiary termowizyjne w praktyce [in Polish], PAK, Warszawa 2004.
6. Wytyczne – Pomiary w elektroenergetyce [in Polish], vol. VIII. COSiW Warszawa & KS KRAK Kraków 2007.
7. Markiewicz H.: Urządzenia elektroenergetyczne [in Polish], WNT, Warszawa 2005.
8. Lisowska-Lis A.: Thermographic monitoring of the power transformers. Measurement Automation Monitoring, vol. 63(4), 154-157, 2017.
9. Witos F., Olszewska A., Opilski Z., Lisowska-Lis A., Szerszeń G.: Application of Acoustic Emission and Thermal Imaging to Test Oil Power Transformers. Energies 13, 5955, 2020.

10. A. Lisowska-Lis: Thermographic and Electrical Test of Medium Voltage Surge Arresters, Measurement Automation Monitoring vol. 65, no. 2, 60-63, 2019.
11. Florkowska B., Moskwa S., Nowak W., Włodek R., Zydroń P.: Modelowanie procedur diagnostycznych w eksploatacji układów izolacyjnych wysokiego napięcia [in Polish], AGH Kraków 2006.
12. Halliday D., Resnick R.: Walker J.: Fundamentals of Physics. Wiley 2007.
13. Florkowska B., Furgał J., Szczerbiński M., Włodek R., Zydroń P.: Materiały elektrotechniczne. Podstawy teoretyczne i zastosowania [in Polish], AGH Kraków, 2010.
14. Hinrichsen V.: Metal Oxide Surge Arresters in High Voltage Power Systems Fundamentals. Siemens A.G., Berlin 2012.
15. Medium voltage surge arresters – product guide. Siemens A.G., Berlin 2017.
16. ABB Technical information. Physical properties of zinc oxide varistors, ed. 4, 2002.
17. Spaeck-Leigsnering Y., Gjonaj E., De Gersem H., Weiland T., Gießel M., Hinrichsen V.: Investigation of thermal stability for a station class surge arrester. IEEE Journal on Multiscale and Multiphysics Computational Techniques, vol 1, 2016, DOI: 10.1109/JMMCT.2016.2636250.
18. Zydroń P., Bonk M., Fuśnik Ł., Szafrania B.: Wpływ temperatury na parametry warystorów tlenkowych ograniczników przepięć niskiego napięcia badanych metodami spektroskopii impedancyjnej [in Polish]. Przegląd Elektrotechniczny no. 10, 158-162, 2016. DOI: 10.15 199/48.2016.10.38.
19. Więcek B., De Mey G., Strąkowska M., Chatziathanasiou V., Gmyrek Z., Strzelecki M., Chatzipanagiotou P.: Various applications of complex thermal impedance for transient and AC heat transfer analysis. MAM no. 06, 210-214, 2015.
20. Seyyedbarzegar S.M., Mirzaie M.: Thermal balance diagram modelling of surge arrester for thermal stability analysis considering ZnO varistor degradation effect. IET Generation, Transmission & Distribution, Vol.: 10, Iss.: 7, 55, 2016, DOI: 10.1049/iet-gtd.2015.0728
21. Zheng Z., Boggs S.A., Imai T., Nishiwaki S.: Computation of arrester thermal stability. IEEE Trans. Power Deliv., no. 3 vol. 25, 1526–1529, 2010, DOI:10.1109/ TPWRD. 2010.2049163.
22. Spaeck-Leigsnering Y., Gjonaj E., De Gersem H., Weiland T., Giessely M., Hinrichseny V.: Multi-Rate Time Integration for Coupled Electrical and Thermal Modeling of Surge Arresters. Proc. of International Conference on Electromagnetics in Advanced Applications (ICEAA), 2015, DOI:10.1109/ICEAA.2015.7297116
23. Novizon N., Abdul-Malek Z.: Electrical and temperature correlation to monitor fault condition of ZnO surge arrester. Proc. of 3rd Int. Conf. on Information Tech., Computer, and Electrical Engineering (ICITACEE), Oct 19-21st, 2016, Semarang, Indonesia, 182-186, 2016.

24. Chen X., Tian X., Li F.: Research of infrared diagnosed of faults of arrester. Proc. of 2008 Int. Conf. on High Voltage Engineering and Application, Chongqing, China, November 9-13, 2008.
25. Srisukkho Ch., Jirapong P.: Analysis of electrical and thermal characteristics of gapless metal oxide arresters using thermal images. Proc. of the Int. Conf. 8th Electrical Engineering/ Electronics, Computer, Telecommunications and Information Technology (ECTI) Association of Thailand, 677-680, 2011. DOI: 10.1109/ECTICON. 2011.5947930.
26. Xu K., Yuan Z., Zhang J., Ji Y., He X., Yang H.: SF_6 gas infrared thermal imaging leakage detection based on faster-RCNN. Proc. of Int. Conf. on Smart Grid and Electrical Automation (ICSGEA), Xiangtan, China, 36-40. 2019.
27. Catalogue - FLIR infrared cameras for gas detection, accessed 25.02.2020 [at]: http://www.ects.pl/files/uploader/Download/Katalog_kamer_gazowych_pl.pdf